Supplementary Information for
Hydrodynamic trapping and locking of bacteria by phase-space topology

Mingyang Guan,[1] Bowen Ling,[1,2] Enhao Liu,[3,4,5] Guoqian Chen,[6,7] and Zhan Wang[1,2,*]

[1] *Key Laboratory for Mechanics in Fluid Solid Coupling Systems, Institute of Mechanics, Chinese Academy of Sciences, Beijing 100190, China*
[2] *School of Engineering Science, University of Chinese Academy of Sciences, Beijing 100049, China*
[3] *State Key Laboratory of Deep Earth Processes and Resources, Guangzhou Institute of Geochemistry/Guangdong Provincial Key Laboratory of Mineral Physics and Materials, Guangzhou Institute of Geochemistry, Chinese Academy of Sciences, Guangzhou 510640, China*
[4] *Guangdong Research Center for Strategic Metals and Green Utilization, Guangzhou 510640, China*
[5] *University of Chinese Academy of Sciences, Beijing 100049, China*
[6] *Department of Mechanics, Peking University, Beijing 100871, China*
[7] *Key Laboratory of River Basin Digital Twinning of Ministry of Water Resources, National Observation and Research Station of Coastal Ecological Environments in Macao, Macau University of Science and Technology, Macao SAR 999078, China*

SUPPLEMENTARY NOTE 1. UNIFIED SMOLUCHOWSKI MODEL AND ANALYTICAL SOLUTIONS

We consider dilute suspensions of self-propelled elongated swimmers in two-dimensional incompressible flows. Each swimmer is characterized by its position $\boldsymbol{r}$ and orientation $\boldsymbol{p}$, whose stochastic dynamics are governed by

$$\dot{\boldsymbol{r}} = \boldsymbol{v}_f(\boldsymbol{r}) + V_s\boldsymbol{p} + \boldsymbol{\xi}_r, \qquad \dot{\boldsymbol{p}} = \boldsymbol{\Omega}(\boldsymbol{r},\boldsymbol{p}) \times \boldsymbol{p} + \boldsymbol{\xi}_p, \tag{S1}$$

where $\boldsymbol{v}_f$ is the imposed flow, V_s is the swimming speed, and $\boldsymbol{\xi}_r$ and $\boldsymbol{\xi}_p$ are Gaussian white noises. The angular velocity takes the Jeffery form $\boldsymbol{\Omega}(\boldsymbol{r},\boldsymbol{p}) = \boldsymbol{\Omega}_f(\boldsymbol{r},\boldsymbol{p})/2 + B\boldsymbol{p} \times [\boldsymbol{E}\cdot\boldsymbol{p}]$, where $\boldsymbol{\Omega}_f = \boldsymbol{\nabla}\times\boldsymbol{v}_f$ is the local flow vorticity, $\boldsymbol{E} = (\boldsymbol{\nabla}\boldsymbol{v}_f + \boldsymbol{\nabla}\boldsymbol{v}_f^{\mathrm{T}})/2$ is the rate-of-strain tensor, and $B = (\Lambda^2-1)/(\Lambda^2+1)$ is the Bretherton parameter that describes particle shape, with Λ the aspect ratio.

The corresponding Smoluchowski equation for the steady-state probability density $P(\boldsymbol{r},\boldsymbol{p})$ reads

$$\boldsymbol{\nabla}_{\boldsymbol{r}}\cdot\boldsymbol{J}_r + \boldsymbol{\nabla}_{\boldsymbol{p}}\cdot\boldsymbol{J}_p = 0, \tag{S2}$$

where $\boldsymbol{J}_r = (\boldsymbol{v}_f + V_s\boldsymbol{p})P - D_t\boldsymbol{\nabla}_r P$ and $\boldsymbol{J}_p = \dot{\boldsymbol{p}}P - D_r\boldsymbol{\nabla}_p P$ are respective flux density tensors in the position and orientation space, D_t and D_r are respective translational and rotational diffusivities, supplemented by normalization

$$\int_{\boldsymbol{r}}\int_{\boldsymbol{p}} P(\boldsymbol{r},\boldsymbol{p})\ \mathrm{d}\boldsymbol{r}\ \mathrm{d}\boldsymbol{p} = 1. \tag{S3}$$

We decompose the phase space into infinite global spaces $\boldsymbol{Q}$ and confined local spaces $\boldsymbol{q}$, such that the Smoluchowski equation is rewritten as

$$\mathcal{L}_Q P + \mathcal{L}_q P = 0, \tag{S4}$$

where $\mathcal{L}_Q = \boldsymbol{\nabla}_{\boldsymbol{Q}}\cdot\boldsymbol{J}_Q$ and $\mathcal{L}_q = \boldsymbol{\nabla}_q\cdot\boldsymbol{J}_q$ are the equivalent operators, with flux density tensors $\boldsymbol{J}_Q$ and $\boldsymbol{J}_q$ in the global and local spaces, respectively. The global space and corresponding variables can be multi-dimensional.

Define local moments

$$P_k(\boldsymbol{q}) = \int_{-\infty}^{\infty} Q^k P(Q,\boldsymbol{q})\ \mathrm{d}Q, \quad k = 0,1,2,\ldots, \tag{S5}$$

where Q is the corresponding variable (single in the present work) in the global space. We derive the hierarchy moment equations as

$$\mathcal{L}_q P_k = kU_Q P_{k-1} + k(k-1)D_t P_{k-2}, \quad k = 0,\ 1,\ 2,\ldots, \tag{S6}$$

where U_Q is the total velocity along Q and $P_{-2} = P_{-1} = 0$. In general, the n-th order local moment can be expanded as [S1, S2]

$$P_k(\boldsymbol{q},t) = \sum_{i=1}^{\infty} p_{ki}(t)\exp(-\lambda_i t) g_i(\boldsymbol{q}), \tag{S7}$$

where λ_i and g_i are eigenvalues and eigenfunctions for the local operator $\mathcal{L}_q$, and p_{ni} is the coefficients to be determined by initial conditions. In the main text only the steady-state zeroth moment P_0 is required; higher moments follow successively. For asymptotically long times, P_0 asymptotes to P through homogenization [S3]. For this eigenvalue problem, P_0 can be obtained through eigenfunction expansions with bi-orthogonal basis function $\{g_j\}_{j=1}^{\infty}$ and a coefficient vector $\boldsymbol{c}$ determined by the bilinear equation corresponding to $\mathcal{L}_q$ and the normalization condition.

The Smoluchowski equation for confined active particles takes the form of a drift–diffusion equation with activity-dependent boundary conditions. In contrast to classical solute transport problems, the local operator is non-self-adjoint due to active swimming and Robin-type confinement, so standard separation of variables and Sturm–Liouville theory cannot be directly applied [S2, S4–S7]. For Robin boundary conditions, we have

$$\boldsymbol{J}_r\cdot\boldsymbol{n} = 0, \tag{S8}$$

where $\boldsymbol{n}$ is the unit outward normal vector on the boundary $z = \pm W/2$. The eigenfunctions for Robin boundary conditions in confined Poiseuille flows are solved analytically as

$$\frac{P_R}{\sqrt{2\pi}},\ \frac{P_R}{\sqrt{\pi}}\cos(\frac{n\pi z}{W}),\ \frac{P_R}{\sqrt{\pi}}\cos(m\psi),\ \frac{P_R}{\sqrt{\pi}}\sin(m\psi),\ P_R\sqrt{\frac{2}{\pi}}\cos(\frac{n\pi z}{W})\cos(m\psi),\ P_R\sqrt{\frac{2}{\pi}}\cos(\frac{n\pi z}{W})\sin(m\psi), \tag{S9}$$

where $P_R = \exp\left[V_s \sin\psi(z - W/2)/D_t\right]$ is an exact solution for zero rotational diffusion and flow strength.

In confined two-dimensional rotlet flows $r \in [1, r_m]$, the eigenfunctions for Robin boundary conditions are solved analytically as

$$\frac{P_a}{\sqrt{2\pi}}R_0(r),\ \frac{P_a}{\sqrt{\pi}}\cos(m\psi)R_0(r),\ \frac{P_a}{\sqrt{\pi}}\sin(m\psi)R_0(r),\ \frac{P_a}{\sqrt{2\pi}}R_n(r),\ \frac{P_a}{\sqrt{\pi}}\cos(m\psi)R_n(r),\ \frac{P_a}{\sqrt{\pi}}\sin(m\psi)R_n(r), \tag{S10}$$

where $P_a = \exp\left(V_s \cos\psi\ r/D_t\right)$ is an exact solution for zero rotational diffusion and flow strength (see **Extended Data Figs.** 4 to 6 for numerical validation), and the radial eigenfunctions are

$$R_0(r) = \sqrt{\frac{2}{r_m^2 - 1}}, \quad R_n(r) = D_n\left[Y_1(k_n)J_0(k_n r) - J_1(k_n)Y_0(k_n r)\right], \quad n = 1, 2, 3, \ldots, \tag{S11}$$

where J_0 and Y_0 are zeroth order Bessel functions of the first and second kind, and J_1 and Y_1 are first order Bessel functions of the first and second kind. The wavenumbers k_n are the positive roots of the transcendental equation

$$\frac{\mathrm{d}}{\mathrm{d}r}R_n(r_m) = 0 \Rightarrow J_1(k_n)Y_1(k_n r_m) - J_1(k_n r_m)Y_1(k_n) = 0, \quad n = 1, 2, \ldots \tag{S12}$$

which ensure the Neumann boundary conditions

$$\left.\frac{\mathrm{d}R}{dr}\right|_{r=1} = 0, \quad \left.\frac{\mathrm{d}R}{dr}\right|_{r=r_m} = 0. \tag{S13}$$

The normalization constant D_n is chosen so that:

$$\int_1^{r_m} R_n^2(r)\ r\ \mathrm{d}r = 1. \tag{S14}$$

The steady state is constructed by factoring out the exact advective equilibrium, reducing the problem to a Neumann Laplacian eigen-expansion for the residual field. The resulting Robin basis naturally encodes the coupling between position and orientation.

For periodic boundary conditions where anti-symmetric parabolic flow profiles repeat periodically with alternating sign [S8], we impose natural conditions in ψ as

$$P|_{\psi=0} = P|_{\psi=2\pi}, \quad \left.\frac{\partial P}{\partial\psi}\right|_{\psi=0} = \left.\frac{\partial P}{\partial\psi}\right|_{\psi=2\pi} \tag{S15}$$

and periodicity at the walls $z = \pm W/2$. The eigenfunctions for these anti-symmetric boundary conditions are solved analytically as

$$\frac{1}{\sqrt{2\pi}},\quad \frac{1}{\sqrt{\pi}}\sin(m\psi),\quad \frac{1}{\sqrt{\pi}}\cos(m\psi),\quad \frac{1}{\sqrt{\pi}}\cos(\frac{2n\pi z}{W}),\quad \frac{1}{\sqrt{\pi}}\sin(\frac{2n\pi z}{W}),$$
$$\sqrt{\frac{\pi}{2}}\cos(\frac{2n\pi z}{W})\sin(m\psi),\ \sqrt{\frac{\pi}{2}}\cos(\frac{2n\pi z}{W})\cos(m\psi),\ \sqrt{\frac{\pi}{2}}\sin(\frac{2n\pi z}{W})\sin(m\psi),\ \sqrt{\frac{\pi}{2}}\sin(\frac{2n\pi z}{W})\cos(m\psi), \tag{S16}$$

with $n = 1,\ 2,\ \ldots$ and $m = 1,\ 2,\ \ldots$.

SUPPLEMENTARY NOTE 2. GENERALIZED VON MISES SOLUTIONS: PASSIVE SCALARS IN ROTLET FLOW AND MICRO-SWIMMERS WITHOUT FLOW

For passive particles $V_s = 0$ in a two-dimensional rotlet flow, the steady-state Smoluchowski equation can be reduced to $\partial_\psi \left[\omega(1+B\cos 2\psi)P/r^2\right] + \left(1+D_t/r^2\right)\partial_{\psi\psi}P = 0$. This equation still has r-dependence through ω/r^2, which acts as a constant at fixed r. Let the probability flux be constant or the angular integration with regard to ψ gives $\left(1+D_t/r^2\right)\partial_\psi P = -\omega(1+B\cos 2\psi)P/r^2$, with general solutions of the form

$$\ln P = -\frac{\omega}{r^2+D_t}\left(\psi + \frac{B}{2}\sin 2\psi\right). \tag{S17}$$

To ensure periodicity in ψ, we give an approximate solution as

$$P(r,\ \psi) \sim \exp\left(-\frac{\omega B}{2(r^2+D_t)}\sin 2\psi\right), \tag{S18}$$

or, with proper normalization

$$\int_1^{r_m}\int_0^{2\pi} P\ r\ \mathrm{d}\psi \mathrm{d}r = 1. \tag{S19}$$

This benchmark solution of P is periodic and of physical significance.

This steady-state distribution has the form of a skewed von Mises–like function, shaped by the cosine term arising from Jeffery torques in micro-swimmer dynamics. The distribution peaks at orientations where $\sin 2\psi = -1$, namely $\psi = 3\pi/4$ and $\psi = 7\pi/4$. These correspond to directions diagonally misaligned with the flow — at 45° counterclockwise from the flow and clockwise from the backward flow. Physically, the shape-induced torque $1+B\cos 2\psi$ rotates particles at different angular velocities depending on their orientation. The steady-state distribution emerges from a balance of (a) slow rotation near orientations that resist torque (where particles linger longer), (b) rapid rotation near unstable orientations (particles quickly rotate through), and (c) rotational diffusion which smooths the distribution. As a result, particles do not align exactly with the flow. Instead, their orientations are biased toward diagonally offset angles, due to the angular dependence of the torque.

As the prefactor $\omega B/r^2$ increases, the orientation distribution becomes increasingly sharp. In the limit $\omega B \gg 1$, Eq. (2) becomes tightly concentrated near $\psi = 3\pi/4$ and $7\pi/4$ corresponding to alignment with the flow direction. However, the distribution never becomes a perfect delta function unless rotational diffusion is entirely absent. On the other hand, the solution fails to capture the main balance mechanism for large ω because the angular profile becomes sharply peaked due to the steep effective potential $U \sim \omega B \sin 2\psi/\left[2(r^2+D_t)\right]$. Moreover, as ω increases, any mismatch between the drift and diffusion operators becomes amplified; the radial diffusion term becomes non-negligible again because the solution has steep angular gradients that indirectly affect radial profiles (e.g., via torque-induced coupling).

The dominance of ω arises from its role in governing the strength of angular advection relative to angular diffusion. In the Smoluchowski equation, the angular drift term scales as $\omega(1+B\cos 2\psi)/r^2$, while angular diffusion scales as $1+D_t/r^2$. Their ratio defines an effective angular Péclet number, $\mathrm{Pe}_\psi = \omega B/(r^2+D_t)$, which controls the sharpness of the angular distribution. The benchmark solution $P(r,\psi) \propto \exp(-\mathrm{Pe}_\psi \sin 2\psi/2)$, is derived by assuming a quasi-equilibrium in ψ, balancing drift and diffusion.

As ω increases, Pe_ψ becomes large, leading to sharply peaked angular distributions that cannot be captured by the single-mode exponential ansatz. In contrast, increasing D_t reduces Pe_ψ, flattening the angular distribution, and making the ansatz more accurate. Therefore, the accuracy of the approximate solution is primarily limited by ω, not D_t, because it directly sets the nonlinearity in r and anisotropy in ψ of the angular flux that the ansatz must approximate.

For the special case without background flows $\omega = 0$, if we assume a small net radial flux for asymptotically long times, the remaining angular governing equations become

$$\left(1+\frac{D_t}{r^2}\right)\frac{\partial^2 P}{\partial\psi^2} + \frac{V_s}{r}\frac{\partial\left(\sin\psi P\right)}{\partial\psi} = 0. \tag{S20}$$

A 1D benchmark solution takes the form

$$P(\psi) \propto \exp\left[\frac{V_s r}{(D_t+r^2)}\cos\psi\right], \tag{S21}$$

with proper normalization as Eq. (S19). Note that this solution violates the Robin boundary condition, and may fail to describe the rotational dynamics when wall accumulation is dominant. The approximation assumes (i) small radial flux everywhere and (ii) mild r-dependence of the angular concentration. Both fail once V_s is large compared to the radial diffusion/geometry scale, so the full r–ψ coupling and boundary layers matter. However, it could be a nice approximation to the orientational distribution averaged over r (see **Supplementary** Fig. S1), where radial nonuniformity near the walls is smoothed through averaging.

The assumptions behind Eq. (S21) break down at large swimming Péclet for the following coupled reasons: (a) The neglected coupling term grows with κ. With $P \propto \exp\left[\kappa(r)\cos\psi\right]$, we have $\partial_r \ln P = \kappa'(r)\cos\psi,\ \kappa'(r) = V_s\,(D_t - r^2)/(D_t + r^2)^2$. The residual of the full equation when we plug this benchmark back in is $\mathcal{R} = V_s \cos\psi \partial_r(rP)/r - D_t\partial_r(r\partial_r P)/r$, because the angular part cancels by construction. Using the expressions above, $\mathcal{R} \sim P\big\{V_s \cos\psi\big[1+r\kappa'(r)\cos\psi\big]/r - D_t\big[\kappa'(r)\cos\psi + r(\kappa''(r)\cos\psi + (\kappa'(r))^2\cos^2\psi)\big]/r\big\}$. For $|\kappa| \gg 1$ (large V_s and/or small D_t over parts of the domain), the terms $\propto \kappa', (\kappa')^2, \kappa''$ become $O(\kappa)$ or larger, so the discarded radial balance is no longer small. (b) Wall accumulation creates boundary layers (Robin boudnary conditions violated). At large V_s, orientations concentrate near $\psi = 0$ (outward) and $\psi = \pi$ (inward). The $\cos\psi$ radial drift then pushes probability to the walls, and a non-negligible radial diffusive flux is required to balance it. That means sharp radial boundary layers form near the walls, which the ansatz cannot capture (and recall that it indeed violates the Robin condition). (c) Strong r-variation of $\kappa(r)$ spoils a single "angular-only" structure. $\kappa(r) = V_s r/(D_t + r^2)$ varies across the gap and even changes slope at $r = \sqrt{D_t}$. For large V_s, the orientational distribution varies dramatically with r, so r-averaging no longer "smooths out" wall effects; instead it mixes very different local von Mises shapes, producing visible deviations from a single von Mises profile.

SUPPLEMENTARY NOTE 3. CONSERVED MOTION AND ORGANIZED PHASE-SPACE SEPARATRICES

We consider the deterministic limit of active particle dynamics in two-dimensional Poiseuille or swirling flows, obtained by setting translational and rotational noise to zero, $D_t = D_r = 0$. In this limit, trapping and escaping are not stochastic processes but are entirely determined by the phase–sparce structure of the underlying dynamical system. Below we show that both planar Poiseuille trapping and two-dimensional rotlet trapping belong to the same class of conserved systems, allowing for a unified quantitative criterion distinguishing captured from escaping trajectories.

Let q denote a generalized transverse coordinate and p an orientational angle. In both geometries considered here,

$$(q,p) = (z,\psi) \quad \text{(Poiseuille)}, \qquad (q,p) = (r,\psi) \quad \text{(rotlet)}, \tag{S22}$$

the deterministic swimmer dynamics may be written in the form

$$\dot{q} = \partial_p H(q,p), \qquad \dot{p} = -\partial_q H(q,p), \tag{S23}$$

where $H(q,p)$ is a conserved quantity along trajectories:

$$\frac{dH}{dt} = 0. \tag{S24}$$

The explicit expression for H depends on the flow geometry and shape anisotropy B, but in both cases it can be constructed analytically. Eq. (S22) implies that the dynamics is integrable and that trajectories are confined to level sets of H in the (q,p) phase space.

The conserved quantity $H(q,p)$ possesses a saddle point (q_s, p_s), corresponding to an unstable fixed point of the deterministic dynamics. The level set

$$H(q,p) = H_c \equiv H(q_s, p_s) \tag{S25}$$

defines a separatrix in the phase space. This separatrix divides phase space into two topologically distinct regions:

1. Closed orbits ($H < H_c$): Trajectories are bounded in q and correspond to deterministic trapping.

2. Open orbits ($H > H_c$): Trajectories exhibit unbounded drift and correspond to escaping.

This separatrix structure is present both in planar Poiseuille and two-dimensional rotlet flows, despite the different functional forms of H.

Planar Poiseuille flows. For a planar Poiseuille flow $u = U(1 - 4z^2/W^2)$ with shear $S = \partial_z u = -8zU/W^2$, the steady-state Smoluchowski equation for the distribution $P(\psi, z)$ reads

$$\frac{\partial P}{\partial t} + \big(u - V_s \cos\psi\big)\frac{\partial P}{\partial y} - V_s \sin\psi \frac{\partial P}{\partial z} + D_r \frac{\partial^2 P}{\partial \psi^2} + \frac{S}{2}\frac{\partial}{\partial \psi}\big[(-1 + B\cos 2\psi)P\big] = 0, \tag{S26}$$

with anti-symmetric periodic boundary conditions at $z = \pm W/2$ so that the parabolic flow profile repeats periodically with alternating sign. For the deterministic limit, we can follow Zottl & Stark [S9] to derive the constants of motion and separatrix. The coupled deterministic ODEs are $\dot{z} = -V_s \sin\psi$, $\dot{\psi} = 4U\, z\,(1 - B\cos 2\psi)/W^2$. Eliminate time

$$\frac{dz}{d\psi} = \frac{\dot{z}}{\dot{\psi}} = -\frac{V_s W^2}{4U}\; \frac{\sin\psi}{z(1 - B\cos 2\psi)}. \tag{S27}$$

Integrating both sides and noting $1 - B\cos 2\psi = 1 - B(2\cos^2\psi - 1) = (1+B) - 2Bu^2$, we obtain (for the usual case $B > 0$) the anti-derivative in terms of arctanh:

$$\frac{z^2}{2} = -\,K\,\Big[\,\operatorname{arctanh}\big(s\cos\psi\big) + C'\Big], \tag{S28}$$

where $s = \sqrt{2B/(1+B)}$, $K = V_s W^2/4U\sqrt{2B(1+B)}$. Equivalently, we write the conserved constant as [S10]

$$h_1(z,\psi) \;=\; \frac{z^2}{2} + K\,\operatorname{arctanh}\big(s\cos\psi\big). \tag{S29}$$

The separatrix in the (z,ψ) plane is the trajectory through the saddle equilibrium at $(z,\psi)=(0,0)$ (or $(0,\pi)$ for the symmetric branch). Evaluate H at the saddle $(0,0)$: $H_{\text{saddle}} = -K\ \text{arctanh}(s)$. Set $H(z,\psi)=H_{\text{saddle}}$. Rearranging gives the separatrix implicitly:

$$\frac{z^2}{2} = K\Big[\text{arctanh}(s\cos\psi) - \text{arctanh}(s)\Big]. \tag{S30}$$

This formula defines the two branches of the separatrix which emanate from $(0,0)$ (and the symmetric one from $(0,\pi)$ if we replace $\cos\psi$ by $\cos(\psi-\pi) = -\cos\psi$).

Linearize the (z,ψ) system about the equilibrium $(z,\psi)=(0,0)$. For small ψ and small z, $\dot z \approx -V_s\psi$, $\dot\psi \approx 4U\,(1-B)\,z/W^2$. Linear system matrix ($\dot a = Aa$) reads

$$A = \begin{pmatrix} 0 & -V_s \\ 4\frac{U}{W^2}(1-B) & 0 \end{pmatrix}. \tag{S31}$$

Its eigenvalues satisfy $\lambda^2 = 4UV_s(1-B)/W^2$, so $\lambda = \pm\sqrt{4UV_s(1-B)/W^2}$.

If $1-B>0$ (i.e. the usual case for prolate swimmers with $0 \le B < 1$), the eigenvalues are real and of opposite sign — $(0,0)$ (and $(0,\pi)$) are saddle points (hyperbolic). That means the rheotactic orientations $\psi = 0,\pi$ at the channel centerline are unstable along one direction (they have stable and unstable manifolds: trajectories approach along one direction and depart along the other). The separatrix we wrote is exactly the stable/unstable manifold boundary between different qualitative trajectory types (see **Supplementary** Fig. S2 for different initial conditions and shear strengths). If $1-B<0$ then eigenvalues are imaginary, i.e. center (neutrally oscillatory).

In summary, for common prolate swimmers ($0 < B < 1$) the centerline rheotactic orientations $\psi = 0$ (upstream) and $\psi = \pi$ (downstream) at $z = 0$ are saddle-type equilibria: they are not simply stable attractors. A swimmer exactly at $(0,0)$ stays aligned, but any generic small perturbation will typically move it off the centerline along the unstable manifold, so there is no robust rheotactic trapping at these orientations. The separatrix expression above separates trajectories that loop in (z,ψ) from those that swing/escape; it also fixes where cusps or turning points occur (these come from the separatrix geometry where $\partial z/\partial\psi$ diverges). If $B \to 0$ (spherical swimmer), simplify $s \to 0$ and the arctanh expansion recovers classical expressions in Ref. [S9].

Rotlet flows. In a rotlet flow, using length scale R and time scale ω^{-1}, and defining the non-dimensional swimming speed $\alpha = V_s/\omega R$, the dimensionless equations of motion take the form

$$\begin{aligned} \dot r &= \alpha\cos\psi, \\ \dot\phi &= \frac{\alpha}{r}\sin\psi + \frac{1}{r^2}, \\ \dot\psi &= -\frac{1}{r^2}(1+B\cos 2\psi) - \frac{\alpha}{r}\sin\psi. \end{aligned} \tag{S32}$$

Specifically for spherical particles ($B=0$), if we define

$$h = \alpha r\sin\psi + \ln r, \tag{S33}$$

Conservation requires

$$\begin{aligned} \dot h &= \alpha\dot r\sin\psi + \alpha r\cos\psi\dot\psi + \frac{\dot r}{r} = \alpha^2\sin\psi\cos\psi + \alpha r\cos\psi\Big(-\frac{1}{r^2} - \frac{\alpha}{r}\sin\psi\Big) + \frac{\alpha\cos\psi}{r} \\ &= \alpha^2\sin\psi\cos\psi - \frac{\alpha\cos\psi}{r} - \alpha^2\sin\psi\cos\psi + \frac{\alpha\cos\psi}{r} = 0. \end{aligned} \tag{S34}$$

Next, we notice that

$$\frac{\dot r^2}{2} + \frac{\alpha^2}{2}\left[\left(\frac{h-\ln r}{\alpha r}\right)^2 - 1\right] = 0. \tag{S35}$$

Thus r behaves as if it was under the influence of an effective potential

$$V(r) = \frac{1}{2}\left[\left(\frac{h-\ln r}{r}\right)^2 - \alpha^2\right], \tag{S36}$$

with an energy-like quantity $E = \dot{r}^2/2 + V(r) \equiv 0$ for all times. Since the effective potential V has limits $V \to -\alpha^2/2$ as $r \to \infty$ and $V \to +\infty$ as $r \to 0$, the entrapment relies on the existence of a local maximum of $V(r) > 0$ to prevent the swimmer from escaping to infinity. Taking the derivative, we see that the condition $dV/dr = 0$ is equivalent to $r = \exp(h)$ or $r = \exp(1+h)$. At $r = \exp(h)$ we have a minimum of the potential, with $V_{\min} = -\alpha^2/2$ while at $r = \exp(1+h)$ there is a local maximum $V_{\max} = \left(e^{-2(h+1)} - \alpha^2\right)/2$. Thus, we predict theoretically that the swimmer will be trapped if and only if $r_0 < \exp(-1-h)$ and $V_{\max} > 0$ so that $h < -1 - \ln\alpha$. The fixed point $(1/\alpha, 3\pi/2)$ is a saddle point, which determines exactly the maximum radius from which trapping could happen.

For elongated particles ($B > 0$), Tanasijevic & Lauga [S11] obtained a conserved quantity

$$h_2 = \frac{\gamma K_0(\eta) + \sin\psi K_1(\eta)}{\gamma I_0(\eta) - \sin\psi I_1(\eta)} \tag{S37}$$

where $\eta = \sqrt{2B(1+B)}/(V_s r)$, $\gamma = \sqrt{(B+1)/(2B)}$, and I, K are the modified Bessel functions of the first kind. We come to a conclusion that a swimmer will be trapped in a 2D rotlet if and only if initially $r_0 < r_c = (1-B)/V_s$ and $h_2(r_0, \psi_0) < h_c(r_c)$, where $h_c = (\gamma K_0 - K_1)/(\gamma I_0 + I_1)$ is the minimum of h_2 evaluated at $r = r_c$.

Despite their different geometries, planar Poiseuille flow and rotlet flow admit a unified Smoluchowski description. In both cases, gradients of shear or vorticity generate a deterministic coupling between swimmer orientation and position, yielding an integrable two-dimensional phase space with conserved invariants. These invariants define separatrices that provide a deterministic explanation for depletion layers in Poiseuille flow and trapping in vortical flows.

SUPPLEMENTARY NOTE 4. 3D VORTICAL FLOWS NEAR A FLAT PLATE AND LOCAL AZIMUTHAL DRIFT

3D vortical flows generated by a rotating sphere near a flat plate. We consider a rigid sphere of radius R rotating with a constant angular velocity $\boldsymbol{\omega}$ in an otherwise quiescent, incompressible Newtonian fluid of viscosity μ. At low Reynolds numbers, $\mathrm{Re} = \rho\omega R^2/\mu \ll 1$, the flow obeys the steady Stokes equations $-\nabla p + \mu\nabla^2\boldsymbol{u} = 0,\ \nabla\cdot\boldsymbol{u} = 0$, subject to no–slip at the particle surface and vanishing velocity at infinity, $\boldsymbol{u}(r = R) = \boldsymbol{\omega}\times\boldsymbol{r},\ \boldsymbol{u}(r\to\infty) = 0$. Because the sphere undergoes pure rotation without translation, the induced flow is purely toroidal. By symmetry, the velocity field can be written in the rotlet form $\boldsymbol{u}(\boldsymbol{r}) = f(r)\,(\boldsymbol{\omega}\times\boldsymbol{r})$, which is divergence-free by construction. The anti-symmetry of the flow implies a spatially uniform pressure, which may be set to zero. Substitution into the Stokes equation yields $\nabla^2\boldsymbol{u} = 0$, leading to the ordinary differential equation $f''(r)+4f'(r)/r = 0$. Imposing decay at infinity and no-slip at $r = R$ gives $f(r) = R^3/r^3$, so that the velocity field reads

$$\boldsymbol{u}(\boldsymbol{r}) = \frac{R^3}{r^3}\,(\boldsymbol{\omega}\times\boldsymbol{r}). \tag{S38}$$

This is the classical rotlet flow, corresponding to the fundamental Stokes solution generated by a point torque. The flow is purely azimuthal, decays as $u\sim r^{-2}$, and possesses non-zero vorticity, $\nabla\times\boldsymbol{u} = 2R^3\boldsymbol{\omega}/r^3$.

Quasi-two-dimensional reduction and image corrections. In the experiments, particle motion is effectively confined to a thin horizontal layer. Restricting attention to the mid-plane and assuming the rotation axis perpendicular to the plane, the flow reduces to a quasi-2D azimuthal field, $\boldsymbol{u} = u_\phi(r)\,\hat{\boldsymbol{e}}_\phi,\ u_\phi(r) \simeq R^3\omega/r^2$. The reduced decay $u_\phi\sim r^{-2}$ reflects the loss of one spatial dimension upon vertical averaging.

The presence of a solid bottom wall enforces a no-slip condition. To leading order, this effect can be incorporated through a hydrodynamic image system. In the far field ($r \gg R$), the dominant correction arises from a mirror rotlet of opposite sign located at a distance $2R$ below the wall, yielding the approximate form

$$v_f(r) \simeq \frac{R^3\omega}{r^2} - \frac{R^3\omega\, r}{\left[r^2+(2R)^2\right]^{3/2}}, \tag{S39}$$

where the second term cancels the azimuthal velocity at the wall to first order. Higher-order singularities (e.g., stresslets) become relevant only at distances comparable to the particle radius.

Rescaling of azimuthal velocity profiles. Introducing the intrinsic Stokes scales for length and velocity, $\tilde{r} = r/R,\ \tilde{u} = u/R\omega$, the wall-corrected Stokes solution collapses onto a parameter-free form,

$$v_f(\tilde{r}) = \frac{1}{\tilde{r}^2} - \frac{\tilde{r}}{(\tilde{r}^2+4)^{3/2}}. \tag{S40}$$

As a consequence, azimuthal velocity profiles measured for different vortex-core radii collapse onto a single master curve when rescaled by R and $R\omega$, in excellent agreement with experiments (see **Fig.** 5 in the main text).

Mean azimuthal drift with orientational locking to the background flow. A central experimentally accessible quantity is the mean azimuthal velocity of bacterial trajectories around the vortex center. From particle tracking, this corresponds to the lab-frame azimuthal drift $\dot{\phi}$. The local drift velocity of swimmers can be written as $\dot{\phi} = \Omega_\phi(r) + V_s\sin\psi/r$, where $\Omega_\phi(r) = \tilde{u}/r$ is the azimuthal velocity of fluid particles. The mean azimuthal drift at a given radius r is therefore

$$\langle\dot{\phi}\rangle(r) = \int_0^{2\pi}\left[\Omega_\phi(r) + \frac{V_s}{r}\sin\psi\right]P(r,\psi)\,\mathrm{d}\psi, \tag{S41}$$

where $P(r,\psi)$ is the steady-state joint distribution of radial position and relative orientation.

Remarkably, in the limit of strongly elongated (rod-like) axis-symmetric swimmers ($B\to 1$), the angular drift is exactly locked to the background vortical flow, $\langle\dot{\phi}\rangle(r) = \Omega_\phi(r)$, independent of swimming speed V_s and noise strengths, provided the system reaches a steady state. This result follows from a vanishing angular probability flux in the steady-state relative-orientation dynamics. For $B\to 1$, the dominant balance simplifies to $\mathrm{d}/\mathrm{d}\psi[(1+\cos 2\psi)P] = 0$, which leads to a local maximum at $\cos\psi = 0$. In this limit, the orientation distribution collapses onto two rheotactic directions. Hence, at the leading order of weak activity, $P(r,\psi)$ is symmetric about $\psi = \pm\pi/2$ and $\sin\psi$ is anti-symmetric such that $\int_0^{2\pi}\sin\psi\,P(r,\psi)\,\mathrm{d}\psi = 0$. Therefore, active swimming does not generate any systematic correction to the mean azimuthal advection. While activity strongly modifies orientation statistics and angular fluctuations, it cannot renormalize the mean angular drift in this idealised rod-like limit. For finite shape anisotropy ($B < 1$) or strong noise, small deviations from perfect locking may arise, but the leading-order behaviour remains dominated by the background flow.

The exact drift locking,

$$\tilde{u}(\tilde{r}) \simeq \Omega_\phi \tilde{r}/\omega = 1/\tilde{r}^2 - \tilde{r}/(\tilde{r}^2+4)^{3/2}, \tag{S42}$$

is closely analogous to the classical Taylor–Aris dispersion in shear flows, where transverse diffusion and shear dramatically enhance streamwise dispersion while leaving the mean drift fixed by the imposed flow. Here, swimming-induced orientational dynamics plays the role of an additional transverse stochastic process: it enhances angular dispersion and residence-time fluctuations, but the mean azimuthal motion of bacterial trajectories remains determined solely by the vortex flow to the first order.

SUPPLEMENTARY TABLE 1. PARAMETERS USED IN SIMULATIONS AND EXPERIMENTS

Supplementary Table S1. **Simulation parameters used in each figure.** Here, W is the confinement width, R the vortex-core radius, V_s the swimming speed, D_t and D_r the translational and rotational diffusivities, B the alignment strength, S the shear-alignment parameter, ω the angular velocity, and f the rotation frequency.

Figures	W (μm)	R (μm)	V_s (μm s^{-1})	D_t	D_r (rad^2 s^{-1})	B	S (rad^{-1})	ω (rad s^{-1})
Fig. 2a	425	–	50	0	1	0.98	–	–
Fig. 2b	425	–	50	0	1	0.98	10	–
Fig. 3	–	30	25	–	0.1	1	–	40π
Fig. 4a, b	425	–	50	0	0	0.98	10	–
Fig. 4c, d	–	–	0.1	0	0	0.5	–	1
Ext. Fig. 1a	425	–	50	0	1	0.98	–	–
Ext. Fig. 1b	–	30	25	–	0.1	1	–	–
Ext. Fig. 2	–	–	0.1	10	0	1	–	–
Ext. Fig. 3	–	–	0.1	–	0	1	–	1
Ext. Fig. 4	–	–	0.1	1	0	0	–	–
Ext. Fig. 5	–	–	0.1	1	0	0	–	–
Ext. Fig. 6	–	–	0.1	10	0	1	–	–
Suppl. Fig. 1	–	–	0.1	10	0	1	–	–
Suppl. Fig. 2a, d	1	–	1	0	0	0.98	1.1	–
Suppl. Fig. 2b, e	425	–	50	0	0	0.98	1.25	–
Suppl. Fig. 2c, f	425	–	50	0	0	0.98	10	–

Fig. 5 (experimental parameters): *E. coli* (wild type) $f = 20$ Hz; *S. pasteurii* $f = 10$ Hz; *E. coli* (smooth swimming) $f = 20$ Hz.

SUPPLEMENTARY VIDEOS 1–5

Supplementary Video 1 | Shear-induced depletion of *E. coli* around a rotating particle (sessile drop). A rotating nickel particle (radius $R = 24.5, \mu$m, rotation frequency 20 Hz) generates a three-dimensional vortical flow that reorients elongated *Escherichia coli* cells and induces a systematic azimuthal drift. Particle rotation is driven by a uniform rotating magnetic field produced by two orthogonal pairs of Helmholtz coils. The resulting coupled orientation–position dynamics rapidly expels bacteria from the particle vicinity, forming a pronounced depletion zone. A small fraction of bacteria transiently accumulates near the particle surface; this near-surface accumulation is captured by a Robin boundary condition in the continuum model and disappears immediately when rotation ceases, confirming its hydrodynamic origin. Quantitative agreement is shown in **Extended Data Fig.** 3.

Supplementary Video 2 | Processed visualization of Supplementary Video 1. The same experiment as in **Supplementary Video 1**, shown after background subtraction and noise reduction using ImageJ (**Supplementary Fig.** 3). Identical experimental parameters are used, with enhanced visibility of bacterial trajectories and depletion dynamics.

Supplementary Video 3 | Shear-induced depletion of *S. pasteurii* in a sessile drop geometry. A bacterial suspension (*Sporosarcina pasteurii*, volume 10,μL) forms a sessile drop attached upon a microscope glass slide, providing a geometry that minimizes the influence of planar walls. A nickel particle (radius $R = 29.5, \mu$m, rotation frequency 10,Hz) is positioned near the drop nadir by gravity. Despite variations in species-specific and morphological features, the vortical shear flow similarly reorients bacteria and expels them from the particle vicinity. The observed azimuthal drift is consistent with the unified theory, see **Extended Data Fig.** 3.

Supplementary Video 4 | Processed visualization of Supplementary Video 3. The same experiment as in **Supplementary Video 3**, shown after background subtraction and noise reduction using ImageJ ((**Supplementary Fig.** 4).

Supplementary Video 5 | Shear-induced depletion in a pendant drop geometry. A pendant drop of bacterial suspension (*Bacillus subtilis*, volume 10,μL) is attached to a microscope glass slide. A rotating nickel particle (radius $R = 20, \mu$m, rotation frequency 20,Hz) is held near the drop nadir by gravity. As in **Supplementary Videos 1–4**, the vortical shear flow induces bacterial reorientation and azimuthal drift, in agreement with Stokes-theory predictions without image correction.

SUPPLEMENTARY FIGURE S1. COMPARISON OF NO-FLOW BENCHMARK WITH SIMULATIONS AND CONTINUUM THEORY

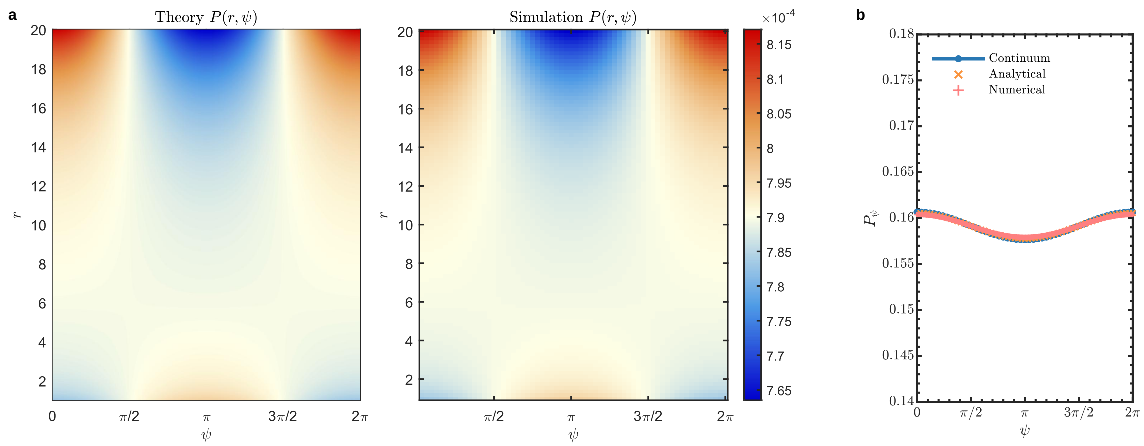

Supplementary Fig. S1. **Steady-state distributions of bacteria in the no-flow case.** **a**, While Eq. (S21) may not depict the overall 2D distributions as the continuum theory does, the 1D analytical solution can well capture the average orientational distribution in **b**.

SUPPLEMENTARY FIGURE S2. SHEAR COMPRESSION OF SEPARATRICES IN VARIOUS SHEAR STRENGTHS

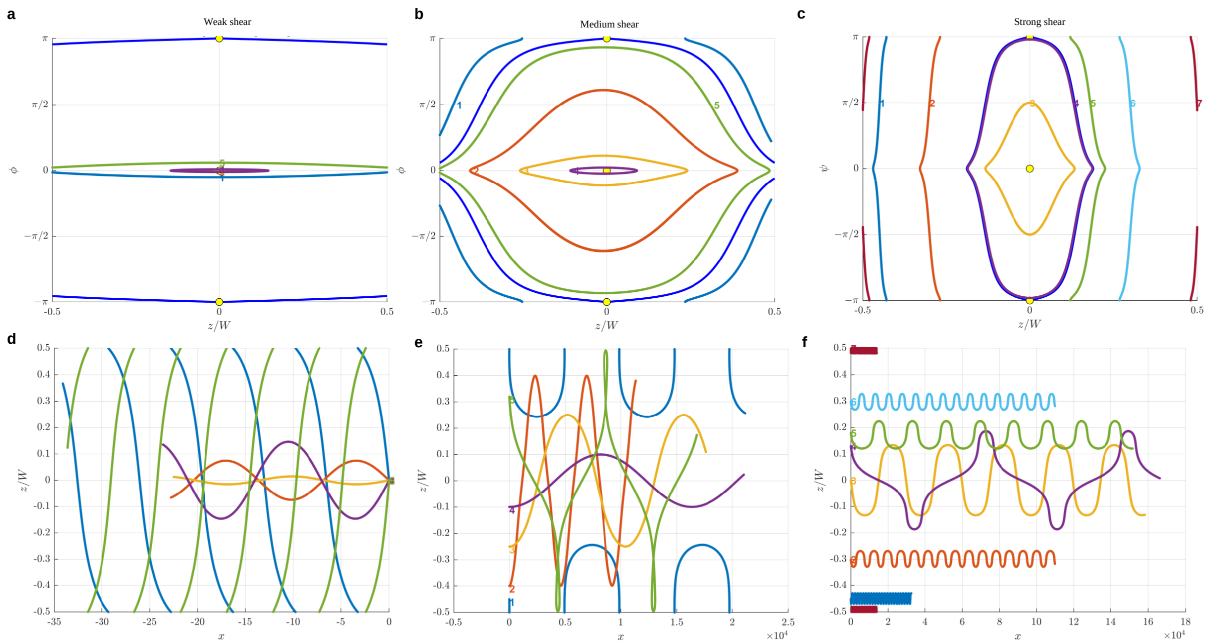

Supplementary Fig. S2. **Deterministic dynamics and separatrices of elongated micro-swimmers under various shear strengths.** Numbers indicate trajectories with different initial conditions and shear strengths. From left to right, the separatices are compressed into eye shapes as the mean shear rate increases.

330 **SUPPLEMENTARY FIGURE S3. EXPERIMENTAL OBSERVATION OF TRAPPED *E. COLI***

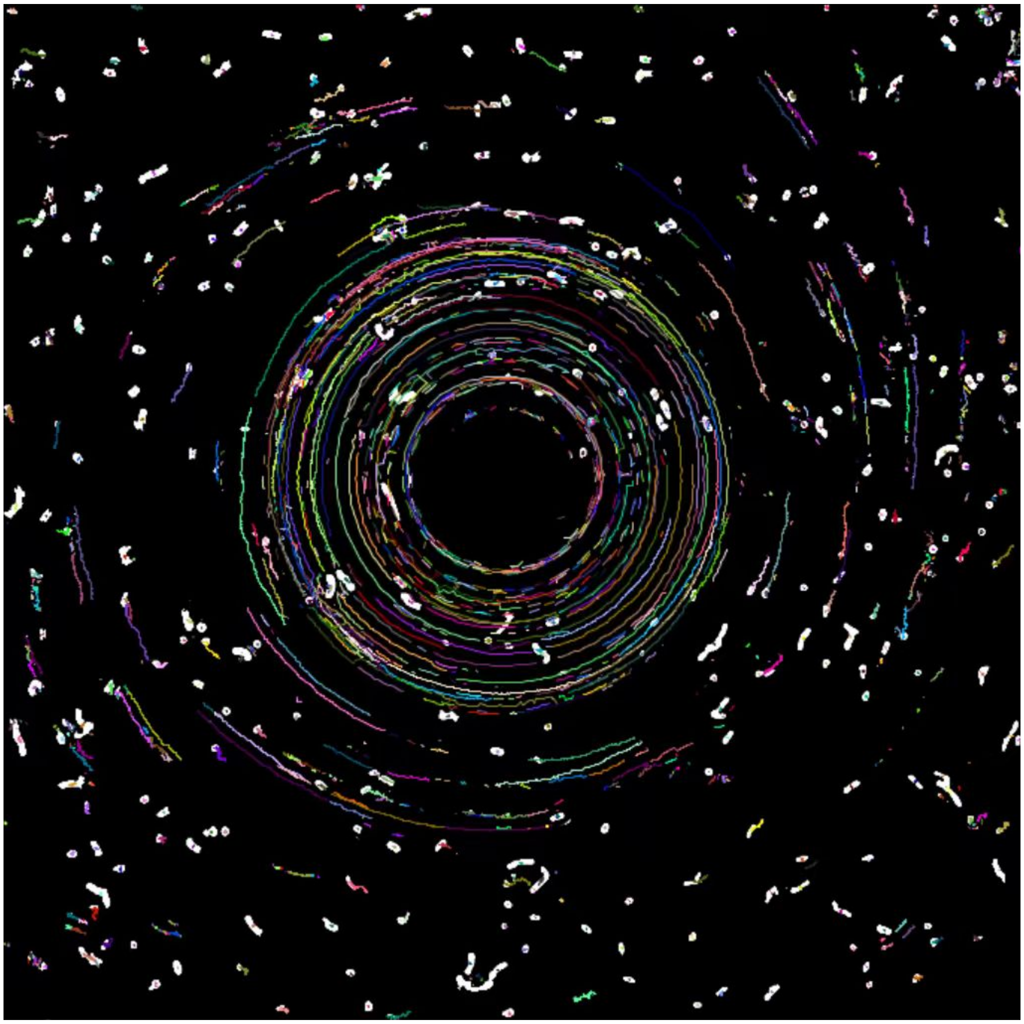

Supplementary Fig. S3. **Formation of hydrodynamic trapping of *E. coli* with orientation locked to the background vortex.** Time-resolved trajectories reveal that bacteria align with and remain phase-locked to the background vortex, leading to persistent trapping and the emergence of a central depletion region. Images correspond to Supplementary Video 2 after background subtraction and noise reduction (ImageJ), with identical experimental parameters.

SUPPLEMENTARY FIGURE S4. REPRODUCIBLE VORTEX-DRIVEN TRAPPING OF *S. PASTEURII*

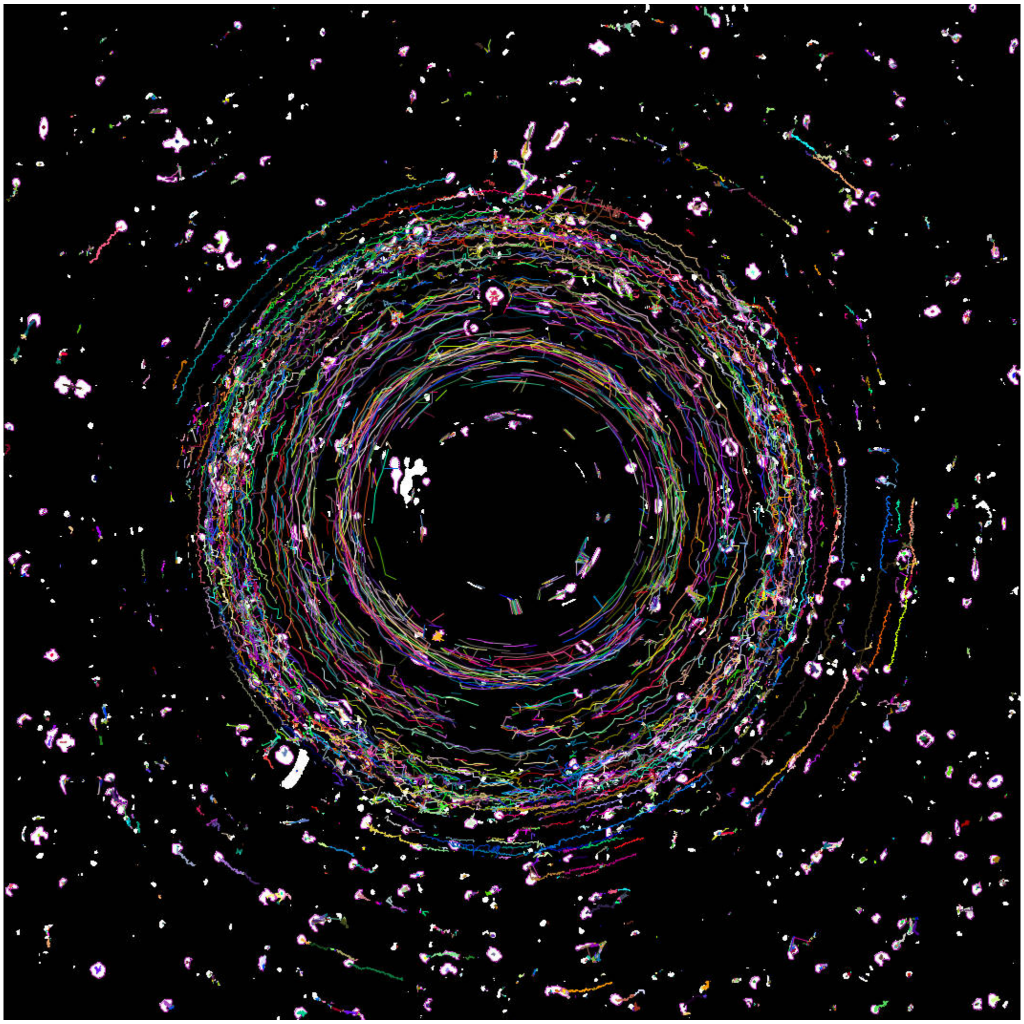

Supplementary Fig. S4. **Cross-species robustness of vortex-induced dynamics.** *S. pasteurii* exhibits the same orientational locking and sustained hydrodynamic confinement observed in *E. coli*, confirming that the depletion dynamics are not species-specific. Images correspond to Supplementary Video 4 after identical post-processing.

SUPPLEMENTARY REFERENCES

* zwang@imech.ac.cn

[S1] N. G. Barton, On the method of moments for solute dispersion, J. Fluid Mech. **126**, 205 (1983).
[S2] W. Jiang and G. Chen, Transient dispersion process of active particles, J. Fluid Mech. **927**, A11 (2021).
[S3] M. Guan, W. Jiang, L. Tao, G. Chen, and J. H. W. Lee, Migration of confined micro-swimmers subject to anisotropic diffusion, J. Fluid Mech. **985**, A44 (2024).
[S4] W. Jiang and G. Chen, Dispersion of active particles in confined unidirectional flows, J. Fluid Mech. **877**, 1 (2019).
[S5] B. Wang, W. Jiang, and G. Chen, Cross-channel distribution and streamwise dispersion of micro-swimmers in a vertical channel flow: A study on the effects of shear, particle shape, and convective inertial torque, Phys. Fluids **34**, 011904 (2022).
[S6] M. Caraglio and T. Franosch, Analytic Solution of an Active Brownian Particle in a Harmonic Well, Phys. Rev. Lett. **129**, 158001 (2022).
[S7] M. Guan, W. Jiang, B. Wang, L. Zeng, Z. Li, and G. Chen, Pre-asymptotic dispersion of active particles through a vertical pipe: The origin of hydrodynamic focusing, J. Fluid Mech. **962**, A14 (2023).
[S8] R. Rusconi, J. S. Guasto, and R. Stocker, Bacterial transport suppressed by fluid shear, Nat. Phys. **10**, 212 (2014).
[S9] A. Zöttl and H. Stark, Nonlinear dynamics of a microswimmer in Poiseuille flow, Phys. Rev. Lett. **108**, 218104 (2012).
[S10] A. Zöttl and H. Stark, Periodic and quasiperiodic motion of an elongated microswimmer in Poiseuille flow, Eur. Phys. J. E **36**, 4 (2013).
[S11] I. Tanasijević and E. Lauga, Microswimmers in vortices: Dynamics and trapping, Soft Matter **18**, 8931 (2022).